NASA TECHNICAL NOTE

NASA TN D-8147

NASA TN D-8147

NOISE LIMITATIONS OF MULTIPLIER PHOTOTUBES IN THE RADIATION ENVIRONMENT OF SPACE

Walter Viehmann and Alfred G. Eubanks

Goddard Space Flight Center
Greenbelt, Md. 20771

NATIONAL AERONAUTICS AND SPACE ADMINISTRATION • WASHINGTON, D. C. • MARCH 1976

1. Report No.	2. Government Accession No.	3. Recipient's Catalog No.
NASA TN D-8147		

4. Title and Subtitle

Noise Limitations of Multiplier Phototubes in the Radiation Environment of Space

5. Report Date: March 1976

6. Performing Organization Code: 755

7. Author(s): Walter Viehmann and Alfred G. Eubanks

8. Performing Organization Report No.: G-7632

9. Performing Organization Name and Address

Goddard Space Flight Center
Greenbelt, Maryland 20771

10. Work Unit No.

11. Contract or Grant No.

13. Type of Report and Period Covered

12. Sponsoring Agency Name and Address

National Aeronautics and Space Administration
Washington, D.C. 20546

14. Sponsoring Agency Code

15. Supplementary Notes

16. Abstract

The contributions of Cerenkov emission, luminescence, secondary electron emission, and bremsstrahlung to radiation-induced dark current and noise of multiplier phototubes are analyzed quantitatively. Fluorescence and Cerenkov emission in the tube window are the major contributors and can quantitatively account for dark count levels observed in orbit. Radiation-induced noise can be minimized by shielding, tube selection, and mode of operation. In the trapped electron and proton environment of the South Atlantic Anomaly, shielding of ≥ 2 g cm^{-2} will eliminate all electrons and protons of $E < 50$ MeV and thereby the major causes of radiation noise. The effects of bremsstrahlung produced in the shielding is negligible compared to fluorescence induced by the remaining protons of $E > 50$ MeV, for which shielding becomes impractical. Optical decoupling of windows and cathode (side-window tubes) leads to further reduction of radiation-induced dark counts, as does reducing the window thickness and effective cathode area, and selection of window/cathode combinations of low fluorescence efficiency. In trapped radiation-free regions of near-earth orbits and in free space, Cerenkov emission by relativistic particles contributes predominantly to the photoelectron yield per event. Operating multiplier phototubes in the photon (pulse) counting mode will discriminate against these large pulses and substantially reduce the dark count and noise to levels determined by fluorescence. To avoid appreciable degradation of signal-to-noise ratio from its photon noise limit under galactic cosmic radiation, photon flux densities at end-window tubes should be kept above $\sim 10^2$ photons cm^{-2}s^{-1} for CsTe cathodes, above $\sim 10^3$ photons cm^{-2}s^{-1} for bialkali cathodes, and above $\sim 10^4$ photons cm^{-2} s^{-1} for trialkali cathodes in the photon counting mode. For analog modes, the corresponding flux densities are approximately 100 times higher for CsTe and bialkali and about 10 times higher for trialkali cathodes. Side-window tubes have an advantage of a factor of 10 over end-window tubes. Minimum desirable photon flux densities in the South Atlantic Anomaly are approximately 5×10^4, 1×10^6, and 5×10^7 photons cm^{-2}s^{-1} for the respective end-window/cathode combinations. Dark count data from a variety of end-window tubes on OAO-3 (Copernicus) and side-window tubes on the Astronomical Netherlands Satellite are in good quantitative agreement with calculations based on fluorescence efficiencies determined in the laboratory.

17. Key Words (Selected by Author(s))	18. Distribution Statement
Multiplier phototubes, Radiation noise, Cerenkov, Fluorescence, Bremsstrahlung, General physics, and Space sciences	Unclassified—Unlimited Cat 74

19. Security Classif. (of this report)	20. Security Classif. (of this page)	21. No. of Pages	22. Price*
Unclassified	Unclassified	29	$3.75

For sale by the National Technical Information Service, Springfield, Virginia 22161

CONTENTS

NOISE LIMITATIONS OF MULTIPLIER PHOTOTUBES IN THE RADIATION ENVIRONMENT OF SPACE

Walter Viehmann and Alfred G. Eubanks
Goddard Space Flight Center
Greenbelt, Maryland

INTRODUCTION

Dark current levels many times in excess of thermionic emission have been observed on multiplier phototubes in space for some time (Young, 1966)*, particularly in the South Atlantic Anomaly (SAA), a distortion of the geomagnetic field with high electron and proton flux densities, and to a lesser—although noticeable—degree outside of the SAA. The resulting dark current and noise degrades both the dynamic range and the photometric accuracy of low-light-level measurements in space (Rogerson et al., 1973). From the observed dependence of the noise level on orbital altitude and position, there appears to be little doubt that energetic particles, ranging from electrons and protons in the SAA to heavy cosmic rays outside the SAA, are the cause of this "background" noise, although the exact mechanisms by which these dark counts are produced and their relative importance have not been quantitatively established.

Energetic particles can create photoelectrons by several mechanisms:

- Expulsion of electrons from the window, cathode, and dynodes (secondary electron emission);
- Cerenkov radiation in the MPT window;
- Luminescence of the MPT window (scintillation); and,
- Indirectly, by causing secondary emission (bremsstrahlung) from the surrounding structures, which, in turn, strikes the tube window, cathode, and dynodes.

In the following, we have attempted to analyze quantitatively each of these mechanisms based on recent laboratory measurements (Viehmann et al., 1975) and data from the literature. Other factors affecting the magnitude of radiation-induced noise, such as tube construction, window material, shielding, and mode of operation (analog versus pulse counting) are also discussed, as are means to minimize radiation noise.

*Also Fowler, W.B., E. I. Reed, and J.E. Blamont, "Effects of Energetic Particles on Photomultiplier Tubes in Earth Orbits up to 1500 km," NASA TM X-63419, Goddard Space Flight Center, 1968.

Recent flight data from a variety of multiplier tubes on OAO-3 (Copernicus) and the Astronomical Netherlands Satellite (ANS) are analyzed in light of the concepts outlined above, and general expressions for signal-to-noise degradation under trapped particle radiation and cosmic radiation are derived.

RADIATION-INDUCED DARK CURRENT: BASIC MECHANISMS AND THEIR EFFICIENCIES

Cerenkov Emission from the MPT Window

Electromagnetic radiation is emitted whenever a charged particle passes through a transparent dielectric of index of refraction, n, with a velocity, $v = \beta c$, greater than the phase velocity, c/n, of light. This "Cerenkov" radiation is emitted perpendicular to a conical surface of halfangle, φ, such that (see figure 1):

$$\cos \vartheta = \sin \varphi = \frac{c/n}{v} = \frac{1}{\beta n} \tag{1}$$

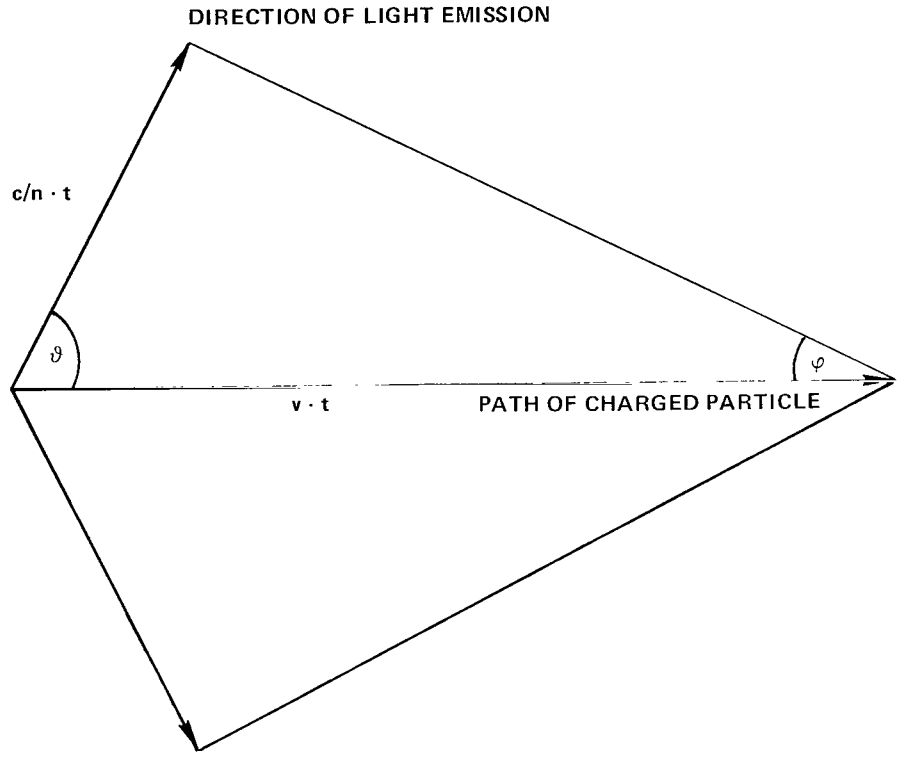

Figure 1. Geometry of Cerenkov emission from charged particle traveling with velocity v in a medium of phase velocity c/n.

The average number of photons emitted per unit pathlength in the wavelength interval between λ_1 and λ_2 is given by (Evans, 1955)

$$\frac{N_{ph}}{\Delta \ell} = \frac{2\pi Z^2}{137}\left(\frac{1}{\lambda_2} - \frac{1}{\lambda_1}\right)\left(1 - \frac{1}{(\beta n)^2}\right) \qquad (2)$$

where Z is the charge number of the particle and $\frac{1}{137}$ is the (dimensionless) fine structure constant.

It is to be noted from equation (2) that the spectral intensity, $\frac{N_{ph}}{\Delta \lambda}$, of Cerenkov radiation

- Is independent of the mass of the particle,
- Is proportional to the square of the particle charge,
- Increases with particle velocity, and
- Is proportional to $\frac{1}{\lambda^2}$, that is, increases quadratically with decreasing (shorter) wavelength.

The useful spectral sensitivity range of multiplier phototubes extends from about 110 nm at the short wavelength limit to about 800 nm at the long wavelength end, with the UV cutoff (λ_1) determined by the window material and the red cutoff (λ_2) set by the photocathode.

The effect of the optical band pass on the number of detectable photons produced by Cerenkov emission from a relativistic ($\beta \sim 1$) electron or proton (Z = 1) is illustrated in figure 2 for a window of 1 mm thickness and index of refraction (n) of 1.5. For the parameters so chosen, the number of photons per Cerenkov event ranges from about 50 for a trialkali cathode on 7056 glass to about 220 for the same cathode on magnesium fluoride or lithium fluoride, with other cathode/window combinations of practical interest giving values in between, such as, for instance, 150 photons per event for CsTe on MgF_2, or for bialkali on fused silica or sapphire, and ~100 for CsI on MgF_2 or LiF, respectively. For future discussions it would be helpful to remember that Cerenkov photons are produced and emitted during a time interval equal to the transmit time of the particle, through the window, that is, within time intervals of the order of 10^{-11} s.

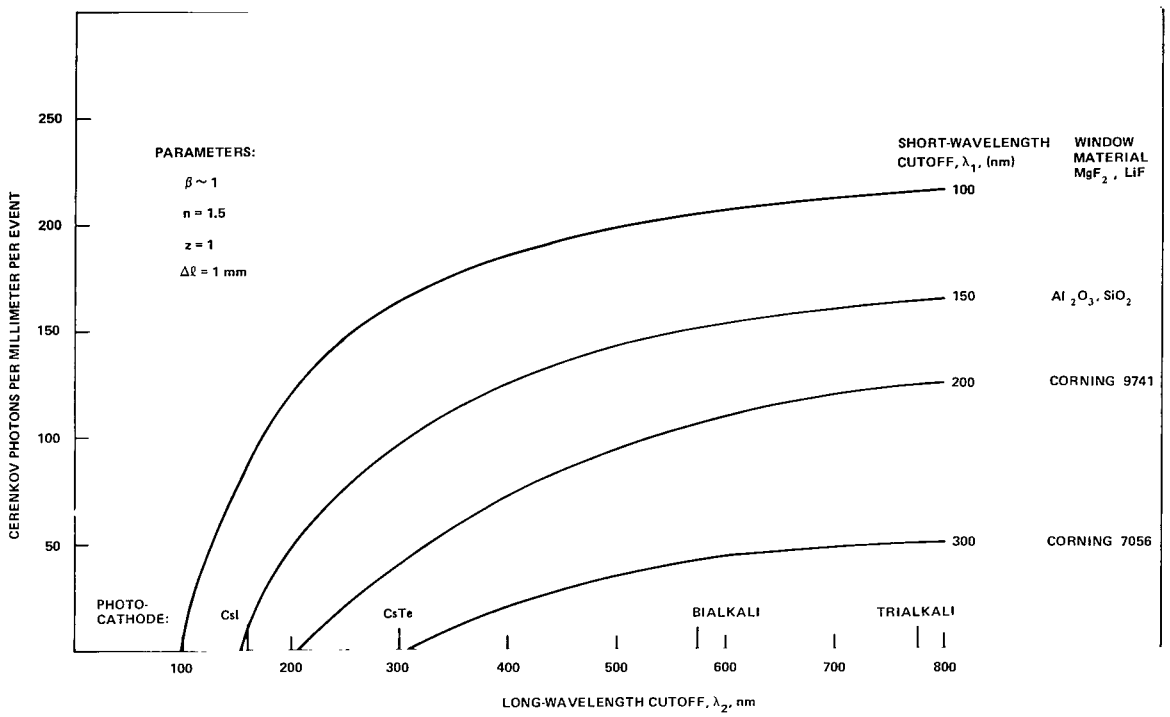

Figure 2. Number of Cerenkov photons produced by a relativistic electron or proton in a 1-mm thick window as a function of long-wavelength cutoff for window materials of different short-wavelength cutoff.

Luminescence of the MPT Window

Fluorescence

The spontaneous emission of visible light from transparent materials under (nonrelativistic) energetic particle irradiation is a familiar phenomenon (Birks, 1964), variously known as cathodoluminescence (in the case of low-energy electron excitation), radioluminescence, or scintillation (for heavy particle and gamma excitation), and it forms the basis for the technique of scintillation counting, used extensively for the detection and characterization of nuclear and space radiation.

The important parameters of scintillator materials are their efficiency, ϵ, and decay time, τ, of the light emission process. The most efficient inorganic scintillator crystals, such as thallium-activated sodium iodiode or cesium iodide, produce about $4 \cdot 10^4$ visible photons per MeV of deposited energy, and their decay times of emission are about 0.25 μs and 1.5 μs, respectively (Birks, 1964). Considerably longer decay times of several microseconds, and sometimes milliseconds, are frequently encountered in inorganic crystals (*Luminescence in Inorganic Solids,* 1966).

Extensive measurements on high-purity (UV-grade) crystalline and amorphous MPT window materials under beta irradiation from an $Sr^{90} - Y^{90}$ source (0 to 2.2 MeV electrons) (Viehmann et al., 1975) have shown that these materials fluoresce in the visible and near UV with characteristic spectral distributions of photon intensities. Their efficiencies extend from typically 10^2 photons per MeV for fused silica (about 0.2 percent that of NaI (Tℓ)) to $\sim 5.10^3$ photons per MeV (about 10 percent that of NaI (Tℓ)) for CaF_2 and BaF_2, when integrated over the wavelength range extending from their respective UV cutoffs to the sensitivity limit of an S-20 photocathode. (Consult table 2 of Viehmann et al., 1975, for details.) For a particle of specific energy loss, (dE/dx), passing through a multiplier phototube window along the pathlength $\Delta\ell$, the number of fluorescence photons is given by (Viehmann et al., 1975)

$$\frac{N_{ph}}{event} = \epsilon_{ph} \cdot \frac{dE}{dx} \cdot \Delta\ell \qquad (3)$$

where ϵ_{ph} is the photon yield per MeV, or efficiency, as defined above, and the specific energy loss dE/dx, is a function of particle energy. Figure 3 gives these functions for electrons, protons, and alpha particles in silicon. With increasing energy dE/dx decreases to a quasi-energy independent value for minimum-ionizing (relativistic) particles which is proportional to Z^2, where Z is the charge of the particle in units of the proton.

As in the case of Cerenkov radiation, the number of fluorescence photons per event is proportional to Z^2 and to $\Delta\ell$. Unlike Cerenkov radiation, however, the spectral distribution of fluorescence emission is not a monotonic function of λ, but rather a material-characteristic spectrum, usually consisting of several broad emission bands whose relative and absolute intensities vary from sample to sample of a given material (Viehmann et al., 1975). For practical purposes, therefore, the fluorescence efficiencies, or photon yields per MeV, are given in Viehmann et al., 1975, for three different photocathodes of different spectral response curves, namely, a CsTe cathode (100 nm $\leqslant \lambda \leqslant$ 300 nm), a bialkali cathode (130 nm $\leqslant \lambda \leqslant$ 430 nm), and an S-20 (trialkali on 7940) cathode (320 $\leqslant \lambda \leqslant$ 570 nm), where the bracketed λ values are those at which the quantum efficiencies are 50 percent of their respective peak values.

Bearing this understanding in mind, we present, in figure 4 as a function of the long wavelength cutoff, the number of fluorescence photons per event for a relativistic particle passing perpendicularly through a 1-mm thick window of six commonly used materials and compare them to the number of Cerenkov photons produced by the same particle. (We neglect small differences due to different indices of refraction and slightly different specific energy losses in the different materials.) As one might expect on the basis of their respective spectral

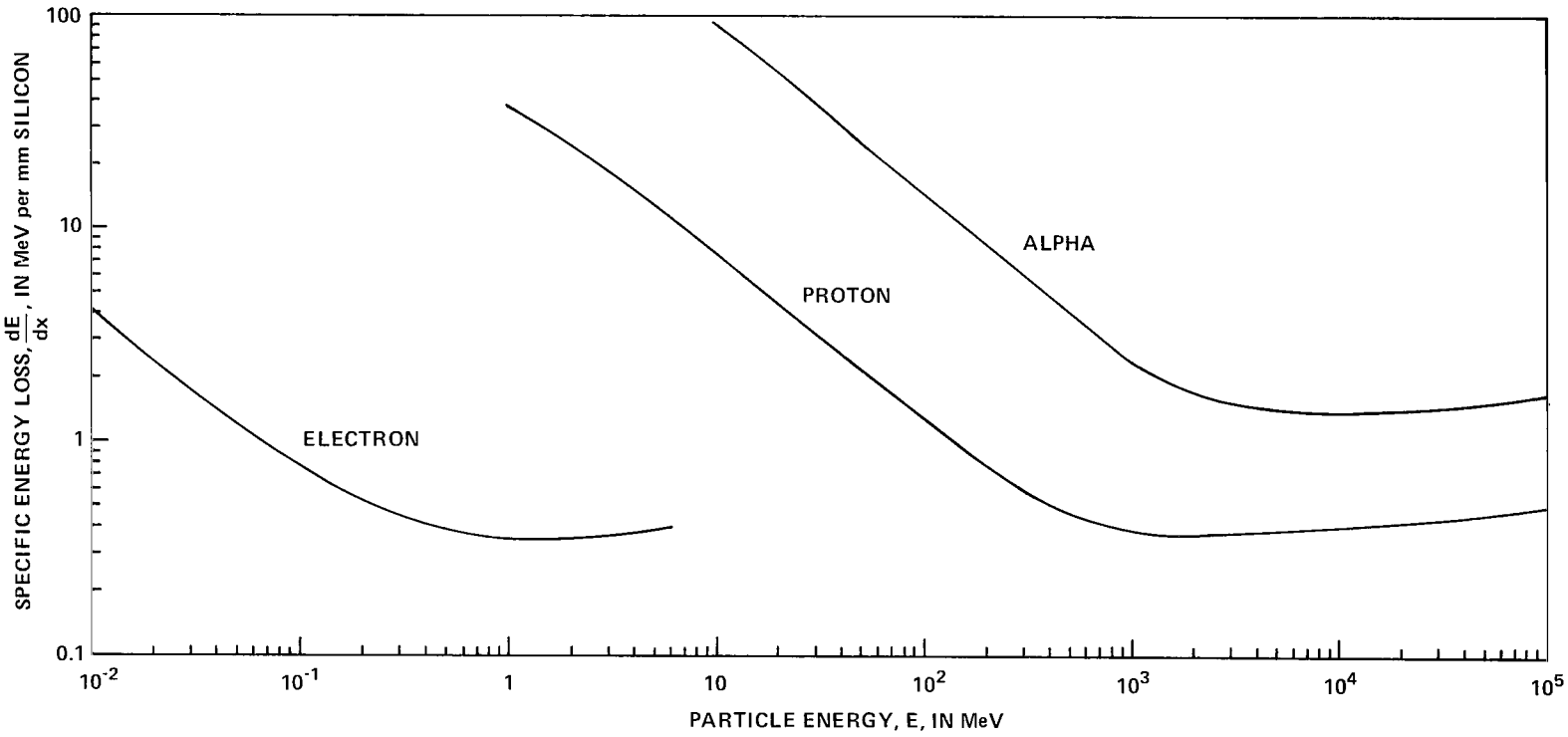

Figure 3. Specific energy loss of electrons, protons, and α-particles in silicon as a function of particle energy.

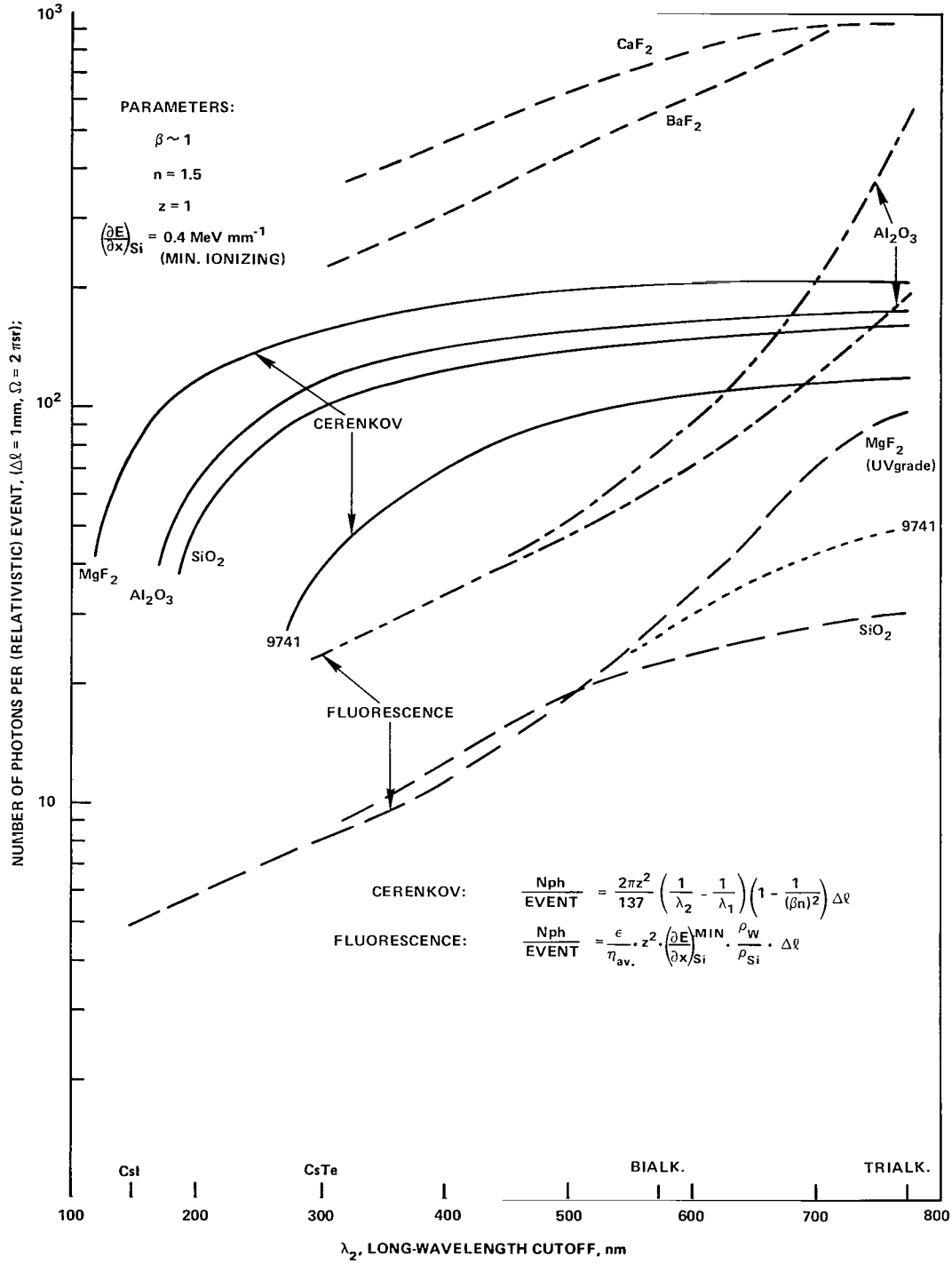

Figure 4. Number of Cerenkov photons and fluorescence photons produced by a relativistic electron or proton in 1-mm thick windows of various materials as a function of long-wavelength cutoff (photocathode).

distributions, Cerenkov radiation is the dominant component in the extreme UV range (CsI, CsTe) for all but the most efficient fluorescent materials (CaF_2 or BaF_2), being about a factor of 10 to 20 more intense than fluorescence in UV window materials, such as MgF_2, fused silica, or 9741 glass. Over the sensitivity range of a bialkali cathode, Cerenkov radiation is about five times more intense than fluorescence in these materials and about twice as intense over the spectral range of a trialkali cathode.

Delayed Fluorescence (Phosphorescence)

Following a radiation dose representative of that experienced in a pass through the SAA, slowly decaying phosphorescence emission occurs in most photomultiplier window materials, with time constants of decay ranging from a few minutes to several days (Viehmann et al., 1975). Laboratory measurements with a 0.4 mCi Sr^{90} - Y^{90} beta source have shown that, for high-quality UV-grade materials, phosphorescence intensities, expressed as a fraction of the steady-state fluorescence intensities, are quite low, ranging from $\sim 2 \cdot 10^{-4}$ for UV-grade MgF_2 to $< 2 \cdot 10^{-6}$ for high-purity fused silica at t = 1 min after removal of the beta excitation (Viehmann et al., 1975). We will see in more detail later that for reasonably well shielded tubes, the phosphorescence-induced dark count rates, after passing through the SAA, represent but a fraction of dark current and noise caused by cosmic-ray-induced fluorescence.

Effects of Bremsstrahlung

Photoelectron pulses induced by Co-60 gamma rays of 1.17-MeV and 1.33-MeV energy have been studied by Dressler and Spitzer (1967) in a variety of multiplier phototubes with various window/cathode combinations. At these γ energies, the predominant interaction of photons with matter is the Compton effect (*American Institute of Physics Handbook*, 1963, Sec. 8), i.e., photon scattering on atomic electrons, resulting in an energetic electron (Compton electron) and a scattered photon of correspondingly lower energy.

For a projected mass of ~ 0.35 to 0.6 g cm^{-2}, which is typical of photocathode windows of 1 to 2 mm thickness, about 1 to 2 percent of the incident Co-60 gamma rays undergo Compton scattering, with an average energy of the recoil electrons of about 0.6 MeV (*American Institute of Physics Handbook,* 1963, Sec. 8). For each electron so produced, a train of pulses was observed, consisting of one major pulse–due to Cerenkov photons produced by the relativistic Compton electrons–and a series of small pulses–due to fluorescence induced in the window by these same electrons through inelastic collisions with atomic electrons of the window material.

Since the measurements by Dressler and Spitzer (1967) were made in a photon-counting mode, the large Cerenkov pulse was counted as just one pulse and the average number of counts (m) per Compton electron thus represents the photoelectrons due to fluorescence emission. Because the range of the Compton electrons is less than the window thickness, it is both legitimate and interesting to convert the m values into fluorescence efficiencies (cts MeV^{-1}, 2π sr^{-1}) and to compare them with values from Viehmann et al., 1975. (See

table 1.) Excepting $CsTe/Al_2O_3$, agreement is quite good, lending credence to the measurements and their interpretation.

Table 1
Fluorescence Efficiencies Deduced from Co-60 γ-Measurements* and from $Sr^{90} - Y^{-90}$ β-Measurements**

Window/Cathode		Fluorescence Efficiency (cts MeV^{-1} 2π sr^{-1})	
		Dressler & Spitzer*	Viehmann et al.**
7056	Bialkali	1.7	2
		2.5	
		5	
7056	Trialkali	8	8
			4
Sapphire	CsTe	17	3
			2
			3
Sapphire	Bialkali	13	26
			22
		90	19
			20
Sapphire	Trialkali	125	120
			87
			26
			200
			28
LiF	CsTe	3.5	2.5
			2.2
			1.7
			3

* Dressler and Spitzer, 1967.
**Viehmann et al., 1975.

From a practical point of view, it is more helpful to express the fluorescence yield, η_γ of γ-rays in photoelectrons (or counts) per photon (γ), per window thickness, as given by

$$\eta_\gamma = \epsilon \cdot \bar{E}_c \cdot \left(1 - \exp -\frac{\sigma_s}{\rho} \cdot t \cdot \rho\right), \tag{4}$$

where ϵ is the fluorescence efficiency in cts $MeV^{-1}\, 2\pi\ sr^{-1}$, $\bar{E}_c$ the average Compton electron energy, σ_s/ρ the mass attenuation coefficient for Compton scattering in $cm^2\, g^{-1}$, t the window thickness in cm, and ρ the density of the window material in g cm^{-3}.

Using data from *American Institute of Physics Handbook*, 1963, and fluorescence efficiencies from Viehmann et al. (1975), we obtain the results given in figure 5. Measured values from Dressler and Spitzer (1967) and by the authors with Co-60, Cs137, and Am 241 sources are included for comparison. The yields so obtained are quite small, due primarily to the low Compton scattering cross sections and concomitant low energy deposition per projected mass (dose rate) of γ-rays, particularly at low γ energies.

Above a γ energy of about 0.5 MeV, the Compton recoil electrons are energetic enough to cause Cerenkov emission. Using equation (2) with Compton scattering coefficients and recoil energies from *American Institute of Physics Handbook*, 1963, Sec. 8), we have computed the Cerenkov contribution to the photoelectron yield of γ rays per millimeter of window thickness for a bialkali cathode of quantum efficiency 0.1 on a MgF_2, Al_2O_3, and 7056 window, respectively (broken curves in figure 5). With a maximum occurring just below 1 MeV, Cerenkov photoelectron yields are about 2 and 5 times as high as fluorescence yields in sapphire and magnesium fluoride or 7056 glass, respectively. They are negligible for γ energies below 0.5 MeV and about equal to the fluorescence yields for 2- to 3-MeV gammas.

Secondary Electron Emission from Cathode, Window, and Dynodes

The emission of secondary electrons under low-energy (<1 keV) electron impact has been studied extensively because of its technological importance in the multiplier stages of MPT's and other photoelectron devices. The secondary electron yield, i.e., the number of secondary electrons per primary electron, is a function of the energy of the primary electron. In general, the yield is less than one for low energies, increases to above unity with increasing energy, goes through a maximum, and decreases again to 1 or less. Maximum yields are of the order of 1 to 2 for metals and 2 to 3 for polycrystalline or amorphous insulating layers, such as SiO_2 or glass (*American Institute of Physics Handbook*, 1963, Sec. 9). Data on secondary electron yield of heavy ions are much less abundant. Yields for ions such as He^{++}, He^+, Ne^+, Ar^+, and Kr^+ on tungsten, molybdenum, or tantalum at energies below 1 keV are all <1, and appear to be proportional to the ionic charge and inversely proportional to the ionic mass (*American Institute of Physics Handbook*, 1963, Sec. 7). This relationship between

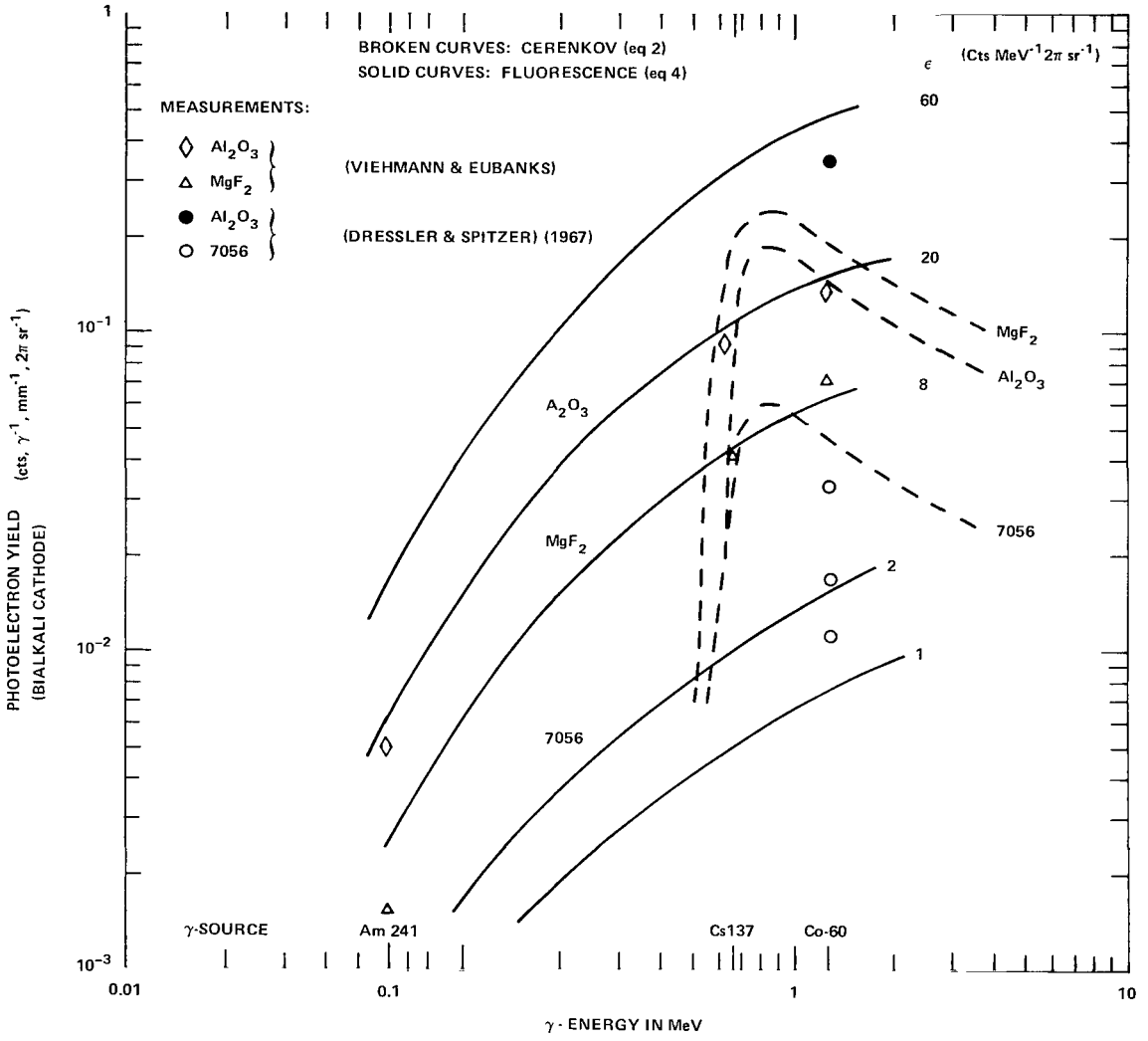

Figure 5. Fluorescence and Cerenkov yields of gamma rays as a function of γ energy for a bialkali photocathode on 1-mm thick windows of various fluorescence efficiencies.

yield and ionic charge (Z) and mass (A) has been investigated by Oda and Lyman (1967) for high energy particles of 6 to 8 MeV/nucleon impinging on Ni foils. In the energy range of interest to the problem at hand (that is, for cosmic rays of $E \gg 10$MeV/nucleon) the yield is a linear function of the specific energy loss according to

$$\eta_s \cong 0.25 \frac{\text{electrons}}{\text{MeV/mm (Si)}} \cdot \frac{dE}{dx} \tag{5}$$

and is about 0.1 for a minimum ionizing proton and ~ 0.4 for a minimum ionizing α-particle. Although comparable measurements on insulators, which would be more representative of MPT windows, are not available, it is probably safe to assume, based on low-energy electron measurements, that their yields would not be different by more than a factor of 2 or 3, i.e., of the order of 1 or less. Except for extreme UV tubes, where cosmic rays produce about 1 to 2 photoelectrons per event by fluorescence (York and Miller, 1974, Viehmann et al., 1975) and somewhat more by Cerenkov emission, the contribution of secondary electron emission to the photoelectron yield thus represents a small correction for bialkali and trialkali tubes, where fluorescence and Cerenkov emission produce many photoelectrons.

OTHER FACTORS AFFECTING RADIATION-INDUCED NOISE

Mode of Operation, Analog Mode versus Pulse Counting

As we have seen in the preceding section, both Cerenkov radiation and fluorescence emission result in many photoelectrons per primary event (figure 3). For tubes operated in dc or charge integration modes, all photoelectrons contribute to the dark current and, therefore, to the noise. The great advantage of the photoelectron counting mode lies not so much in its insensitivity to the numerous small pulses originating at the dynodes (dynode noise) since, because of their small size, they contribute little to the current and negligibly to the noise. The great advantage of pulse counting is that very large pulses are discriminated against. Photoelectrons separated by less than the MPT transit time, which is typically 20 to 40 nanoseconds, are no longer counted as individual pulses (coincidence loss). As the product of instantaneous photoelectron rate, N_{pe}, and transit time, t_R, approaches one, the tube output pulse rate goes through a maximum and then decreases exponentially with increasing input rate according to:

$$\dot{N}_{out} = \dot{N}_{pe} \cdot \exp(-\dot{N}_{pe}\, t_R) \tag{6}$$

For a Cerenkov pulse of typically 20 photoelectrons emitted over a time interval of $\sim 10^{-11}$ s, the instantaneous input rate is of the order of 10^{12} photoelectrons per second so that $\dot{N}_{Pe}^{Ce} \cdot t_R > 10^6$ and $\dot{N}_{out} \rightarrow 0$, that is, the tube is "paralyzed".

Fluorescence emission, on the other hand, takes place over time periods of a microsecond or more so that $\dot{N}_{pe}^{Fl} \cdot t_R \leq 10^{-1}$, resulting in pile-up errors of 10 percent, or less.

Tube Construction: End Window versus Side Window

In end-window multiplier tubes, the cathode is deposited on the window and, therefore, is well coupled to it optically. The majority of photons emanating diffusely from a point in the faceplate into a hemisphere will reach the cathode, a fact that led us to define fluorescence efficiencies, for instance, as the number of counts in a solid angle of 2π sr per MeV of incident particle energy deposited in the faceplate. From the preceding discussions several obvious, although not always practical, possibilities of making a tube less susceptible to radiation-induced noise become apparent:

- Select the least sensitive cathode/window combination commensurate with the spectral band pass required;
- Make the cathode/window area as small as the f-number of the preceding optical system will allow and; therefore
- Use a fast optical system;
- Make the window thinner, which for mechanical reasons is predicated on making its diameter smaller; and
- Decouple the cathode optically from the window.

Of these, the latter is readily available in the form of side-window tubes, in which the cathode is deposited on a metallic substrate remote from the window. The minimum reduction of radiation-induced noise current to be expected from this geometry is given by the ratio $\Omega/2\pi$, where Ω is the solid angle defined by the critical angle for total interval reflection at the window-vacuum interface. Table 2 lists these factors for a number of window materials, and we see that reductions of three to five can be realized from decoupling of window and cathode. Orbital dark count data from the UV spectrophotometer on the Astronomy Netherlands Satellite, which uses side-window tubes of the EMR 641 series and is discussed in more detail below, seemingly support this contention.

Shielding

In near-earth orbits, high particle fluxes are encountered in the SAA, a distortion of the geomagnetic field, which results in higher trapped particle fluxes at lower altitudes than are usually experienced over most of the earth's surface. With flux densities for electrons of $>10^6$ cm $^{-2}$ s^{-1} and $> 10^4$ cm^{-2} s^{-1} for protons, well over 90 percent of the electrons have energies less than 2 MeV and most of the protons have energies less than 5 MeV. However, the tails of the energy distributions extend to $>$ 4 MeV for electrons and $>$ 100 MeV for

protons. Neglecting the effects of bremsstrahlung for the moment, the effect of shielding on the radiation-induced dark count rate due to window fluorescence can be expressed by

$$\dot{N}_{FL} = \phi_{tr} \cdot A \left(\frac{dE}{dx}\right)_{Si} \cdot \frac{\rho_w}{\rho_{Si}} \cdot t \cdot \epsilon \qquad (7)$$

where ϕ_{tr} is the transmitted particle flux density, A, t, and ρ_w are the area, thickness, and density of the MPT window, respectively, ϵ the fluorescence efficiency of the window/cathode combination, and $(dE/dx)_{Si}$ the specific energy loss in silicon.

Table 2
Optical Decoupling Coefficient of Remote Cathodes Due to Total Interval Reflection Losses

Window Material	Index of Refraction	Critical Angle (Total Int. Refl.)	$\frac{\Omega}{2\pi}$
Al_2O_3	1.78	34°	0.17
LiF	1.60	39°	0.22
9741	1.47	43°	0.27
MgF_2	1.38	46°	0.31

Using dE/dx values from figure 3 and taking a somewhat simplified approach by considering normal incidence only and by approximating the effect of the shielding on the energy spectrum of the transmitted particle fluxes by a sharp cut-on at the energy for which the thickness of the shielding equals the range at that particular energy, we obtain the results represented in figure 6 (taken from Viehmann et al., 1975). This figure depicts the dark count rate at the peak of the SAA at 550-km altitude, normalized to a photocathode area of 1 cm^2, a window thickness of 1 mm, and unit fluorescence efficiency, ϵ = 1 count MeV^{-1}, $2\pi sr^{-1}$. In order to facilitate its use for different altitudes, the relative variation of peak flux density at the center of the SAA with orbital altitude is included (see insert on figure 6).

For "moderate" shielding of $\leq$ 5 mm of aluminum, fluorescence-induced counts are predominantly due to electrons, that is, about an order of magnitude greater than those due to protons. It should also be pointed out that electrons of $\gtrsim$ 0.5 MeV (range $\gtrsim$ 1 mm of Al) are energetic enough to cause Cerenkov emission. For a tube operated in analog mode, therefore, 10 to 20 photoelectrons per primary electron per mm of window thickness should

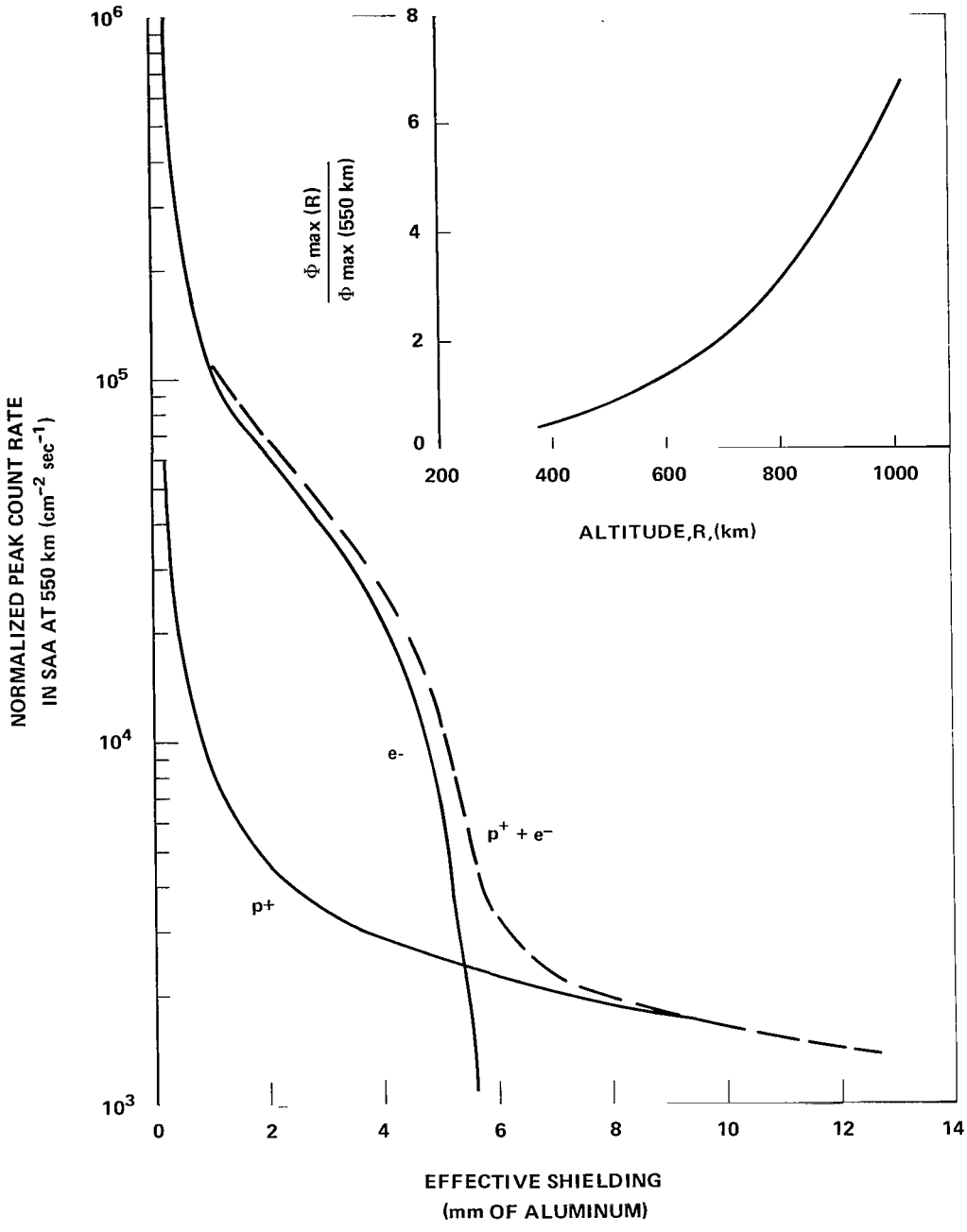

Figure 6. Calculated electron- and proton-induced count rates for peak flux densities at 550 km altitude as a function of effective shielding, normalized to window thickness of 1 mm and fluorescence efficiency of ϵ = 1 count MeV^{-1} 2π sr^{-1}. Insert: Relative variation of peak flux densities of electrons (E > 0.5 MeV) and protons (E > 5 MeV) at the center of the SAA with orbital altitude.

be added. (For most cases of practical interest, for instance, for MgF_2 or SiO_2 with $\epsilon \sim 5$ to 10 cts MeV^{-1} 2πsr^{-1}, this amounts to approximately two to four times the fluorescence component.) More importantly, however, electron-induced dark counts can be avoided

entirely by providing sufficient shielding. Above an effective shielding of approximately 7 mm of aluminum, count rates are entirely due to fluorescence induced by protons of E>40 MeV, which are not energetic enough to cause Cerenkov emission.

Fortunately, the conversion efficiency of electrons into bremsstrahlung is quite low and the bremsstrahlung spectra are peaked toward low energies, where the fluorescence yield of gammas is low and their Cerenkov yield is zero. A typical (differential) electron spectrum and resulting bremsstrahlung spectra behind plane infinite aluminum shields of two different thicknesses are shown in figure 7. These curves were taken from Watts, et al., (1974)*, and scaled to the center of the SAA at approximately 600 km altitude. For a shield thickness of ~7.5 mm of Al (~2g cm^{-2}) the bremsstrahlung yield, defined as

$$\eta_B = \frac{\int_o^\infty N_\gamma(E)\, E_\gamma dE}{\int_o^\infty N_e(E)\, E_e dE} \tag{8}$$

is about $2 \cdot 10^{-3}$ gammas per electron and the bremsstrahlung-induced dark count rate for, say, a bialkali cathode on a 1 mm thick MgF_2 window as given by

$$\overset{\circ}{N}_{Pe}(\gamma) = \int_o^\infty N_\gamma(E)\, E_\gamma\, (\eta_{F\ell} + \eta_{Ce})\, dE \tag{9}$$

is of the order of 200 to 300 photoelectrons per cm^2 per second, or about 1 percent of the proton-induced dark count rate.

FLIGHT DATA AND THEIR INTERPRETATION

The most detailed orbital dark count data available are those of a series of UV and UV/visible sensitive end-window multiplier tubes of the Princeton Experiment Package (PEP) on OAO-3 (Rogerson, et al., 1973; Viehmann, et al., 1975; York and Miller, 1974). The satellite passes through the SAA at 750 km altitude and 35° inclination. Dark count maxima experienced at the center of the SAA are summarized in table 3, together with pertinent parameters of the tubes on which they were observed. Due to limitations in counter capacity, the values listed represent lower limits, as indicated. For ready comparison

*Watts, J.W. Jr., M.O. Burrell, and J.J. Wright, "Charged Particle Environment for the LST," NASA TM X-64858, Marshall Space Flight Center, 1974.

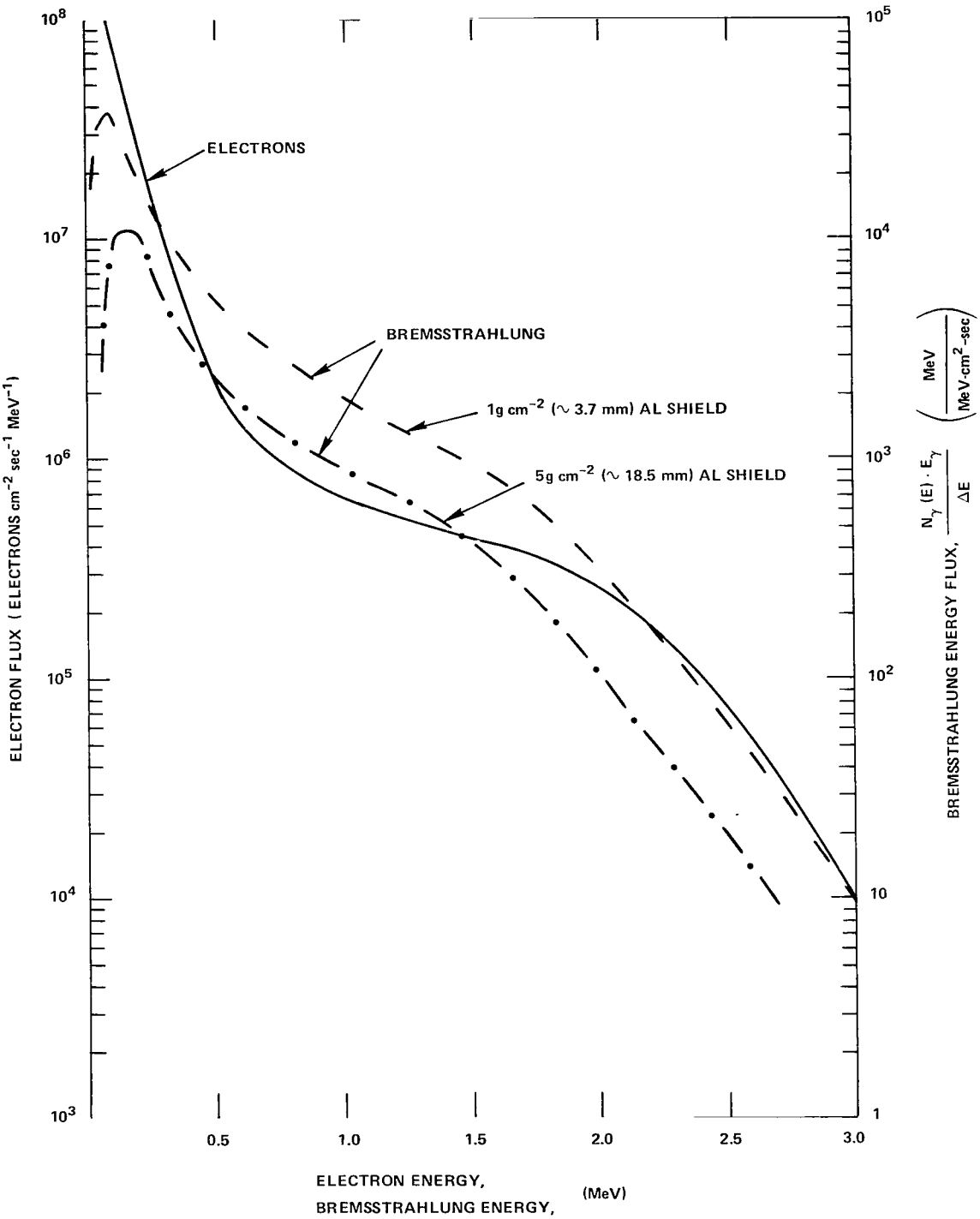

Figure 7. Differential trapped electron spectrum at peak of SAA (~ 600 km) and bremsstrahlung spectrum behind plane infinite aluminum shields of indicated thicknesses resulting from electron flux.

Table 3

Dark Count Rates of OAO-3 Princeton Experiment Package (PEP) Tubes (End-window) and of Astronomical Netherlands Satellite (ANS) Ultraviolet Spectrometer (UVS) Tubes (Side-window) at Peak of SAA and Pertinent Parameters of PMT's on Which They Were Observed

Tube EMR Type	Tube Parameters						Peak of South Atlantic Anomaly (SAA)		
OAO - PEP* (At 750 km Altitude)	Cathode	Window Material	Effective Cathode Area (cm^2)	Window Thickness (mm)	Peak Quantum Efficiency (Nominal)	Typical Fluorescence Yield** Counts MeV^{-1}	Observed Dark Count	Dark Count Rate Per Unit Area ($cm^{-2} s^{-1}$)	Normalized to ϵ = 1 Count MeV^{-1} t = 1 mm 550 km Altitude
V_1 541N-09	Bialkali	MgF_2	1.8	1.0	0.15	20†	$\frac{>10^6}{14s}$	$>4 \times 10^4$	$>0.8 \times 10^3$
V_2 541N-09	Bialkali	MgF_2	1.8	1.0	0.15	10	$\frac{>10^6}{14s}$	$>4 \times 10^4$	$>1.6 \times 10^3$
V_3 541D-01	Bialkali	7056	5.0	1.5	0.06	2	$\frac{>10^6}{14s}$	$>1.4 \times 10^4$	$>2 \times 10^3$
U_3 541G-08	CsI	LiF	0.7	1.0	0.18	1‡	$\frac{>5 \times 10^4}{14s}$	$>5 \times 10^3$	$>2 \times 10^3$
ANS - UVS (At 1,114 km Altitude)									
1 641G-09	CsI	MgF_2	0.7	1.0	0.24	1.5	$\frac{4.8 \times 10^3}{s}$	6.9×10^3	5.7×10^2
2 641F-09	CsTe	MgF_2	0.7	2.0	0.11	1.0	$\frac{5.1 \times 10^3}{s}$	7.2×10^3	4.5×10^2
3 641F-09	CsTe	MgF_2	0.7	2.0	0.11	1.0	$\frac{5.1 \times 10^3}{s}$	7.2×10^3	4.5×10^2
4 641F-03	CsTe	9741	0.7	2.0	0.11	0.7	$\frac{5.4 \times 10^3}{s}$	7.7×10^3	6.9×10^2
5 641N-03	Bialkali	9741	2.0	2.2 (average)	0.24	6.0	$\frac{2.77 \times 10^4}{s}$	1.4×10^4	1.3×10^2

*Rogerson et al., 1973; Viehmann et al., 1975.

**Viehmann et al., 1975, table 2.

†Although V_1 and V_2 are nominally identical, the dark count rate on V_1 is about twice that of V_2; we assign a high value of ϵ = 20 counts MeV^{-1} to V_1 and a more typical value of ϵ = 10 counts MeV^{-1} to V_2.

‡Measured value, not included in table 2 of Viehmann et al., 1975.

with figure 6, peak count rates have been normalized to an altitude of 550 km, a window thickness of 1 mm, and unit fluorescence efficiency by using typical fluorescence efficiencies from Viehmann et al. (1975), for the respective window/cathode combinations. We observe good agreement with calculated values for well-shielded end-window tubes.

A similar analysis of peak dark count data from the ANS-UVS tubes (side-window), which pass through the SAA at approximately 1100 km altitude and considerably higher flux densities, leads to normalized count rates which are about 5 to 10 times lower than those of the PEP end-window tubes, that is, lower by a factor of two than one would expect on the basis of optical decoupling of window and cathode alone, and indicating, perhaps, that, depending on detailed tube construction, additional decoupling results from geometrical limitations of the solid angle subtended by the cathode from a point in the window. However, the shielding of the ANS tubes by 3.2 grams per cm^2 of Kennerium, a tungsten alloy, in addition to the incidental shielding provided by the spacecraft and other payloads, could readily account for a factor of two as well.

Of much greater practical and scientific interest is the radiation-induced noise of MPT's outside of the SAA, where cosmic rays of event rate, r, produce a large number, m, of photoelectrons per event. Although the resulting average dark count rate, $\overset{o}{N}_{av} = rm$, is only moderately higher than thermal dark counts, tubes are noisy because the statistical variance of dark counts accumulated over a counting interval, t, is $m \cdot \overset{o}{N}_{av} \cdot t$, that is, each event of m photoelectrons contributes as much as m^2 thermal photoelectrons to the noise. As discussed in more detail in Viehmann et al. (1975), in low-altitude/low-inclination near-earth orbits, α-particles of an event rate of ~ 0.5 $cm^{-2} s^{-1}$ near the equator and ~ 1.5 $cm^{-2} s^{-1}$ near the poles, and high to medium Z cosmic rays about 1/10 as abundant can quantitatively account for observed count rates and m-values. This is illustrated in table 4, which summarizes dark-count data of the Copernicus tubes observed outside of the SAA for orbits which did not contain a recent pass through the SAA and for which the phosphorescence components have, therefore, decayed. (After passing through the SAA, a slowly decaying phosphorescence component of about 20 cts $cm^{-2} s^{-1}$ can be discerned on the visible tubes, V_1, V_2, and V_3). The data given in table 4 are based on average dark counts and their variances, taken in the photoelectron counting mode with an integration period of 14 seconds, around orbit number 4000. They have been reduced to "orbit zero," because, since launch, the dark counts on the V tubes have increased monotonically with time by factors ranging from 1.5 for V_3 to 1.8 for V_1 and 2.68 for V_2 in orbit 4000 (York and Miller, 1974). This increase is interpreted as a "sensitization" of fluorescence by radiation damage sustained in the SAA, a view which is supported by laboratory results on 1-MeV electron irradiated MgF_2 and LiF samples (Viehmann et al., 1975).

The average number of counts per event ranges from ~ 1 for the windowless FUV tubes (direct interaction of cosmic-ray particles with the cathode, secondary electron emission) to ~ 10 for a bialkali cathode on 7056 glass (V_3) and ~ 100 for bialkali on MgF_2 (V_1).

Table 4
Summary of Dark Count Data for OAO-3 (PEP)* Outside the SAA.**
In Near-earth Orbits He Nuclei and Heavier Cosmic Rays
are Responsible for Enhanced Dark Counts

OAO-3 PEP	Dark Count Rate Per Unit Area (cm^{-2} sec^{-1})		Number of Counts Per Event				
			Calculated				Observed
Tube EMR Type	At Closest Approach to Magnetic Poles	Near Equator	Protons; $E > 10^9$ eV $\frac{dE}{dx}$ = 0.4 MeV mm^{-1}	α-particle; $E > 4 \times 10^9$ eV $\frac{dE}{dx}$ = 1.6 MeV mm^{-1}	Cosmic Rays; A = 6 to 19, Z = 3 to 9 $\frac{dE}{dx}_{av}$ = 18 MeV mm^{-1}	Average for 90% α and 10% CR	Orbital Average Derived from Counting Statistics
U_1 FUV	1.8	0.42	–	–	–	–	1
U_2 FUV	1.35	0.32	–	–	–	–	1
U_3 541G-08 (ϵ = 1 count MeV^{-1})	3	1	0.4	1.6	18	3	>1†
V_1 541N-09 (ϵ = 20 counts MeV^{-1})	139	54	10	40	450	80	100
V_2 541N-09 (ϵ = 10 counts MeV^{-1})	64	22	5	20	225	40	40
V_3 541D-01 (ϵ = 2 counts MeV^{-1})	19	5.7	1.35	5.5	60	11	11

*Corrected to orbit zero.
**York and Miller, 1974; Viehmann et al., 1975.
†Estimated value.

After these data were taken, the integration period for V_1 data has been changed from 14 to 1/8s in order to look at the dark count problem with better time resolution. Examples of typical results so obtained are shown in figure 8 for a "quiet" part of the orbit (left), that is, near the Equator, where the event rate is $\sim 0.5\ cm^{-2}s^{-1}$, and for a noisy period at higher geomagnetic latitudes, where $r \sim 1.5\ cm^{-2}s^{-1}$ (right section of figure 8).

Unlike the data in table 4, the 1/8-s counts have not been reduced to orbit zero, and thus are about twice as high as the reduced data in table 4. Although the time resolution is not as good as one might wish and a detailed analysis of the data will, therefore, not be attempted here, it is probably correct to deduce, particularly for the "quiet" part of the orbit, that at least three groups of "bursts" can be discerned, presumably caused by protons, α-particles, and an occasional heavier cosmic ray particle, with intensity ratios commensurate with the Z^2 dependence of m.

RADIATION-INDUCED SIGNAL-TO-NOISE DEGRADATION

For multiplier phototubes exhibiting Poissonian dynode gain statistics and high first dynode gain, the signal-to-noise ratio is given by

$$SNR = \frac{\eta \dot{N} t}{\sqrt{(\eta \dot{N} + \dot{N}_D) t}} \tag{10}$$

where η is the quantum efficiency, $\dot{N}$ the photon arrival rate, $\dot{N}_D$ the thermal dark count rate, and t the integration time. If the signal photoelectron rate, $\eta\dot{N}$, is large compared to the dark count rate, $\dot{N}_D$, this expression reduces to the so-called photon noise-limited SNR,

$$SNR_{Ph} = \sqrt{\eta \dot{N} t} \tag{11}$$

that is, the "noise in signal" is solely determined by the statistical nature of the photon flux and is equal to the standard deviation

$$\sigma = \sqrt{\eta \dot{N} t} \tag{12}$$

of the (Poissonian) distribution of photoelectron counts accumulated over a time t.

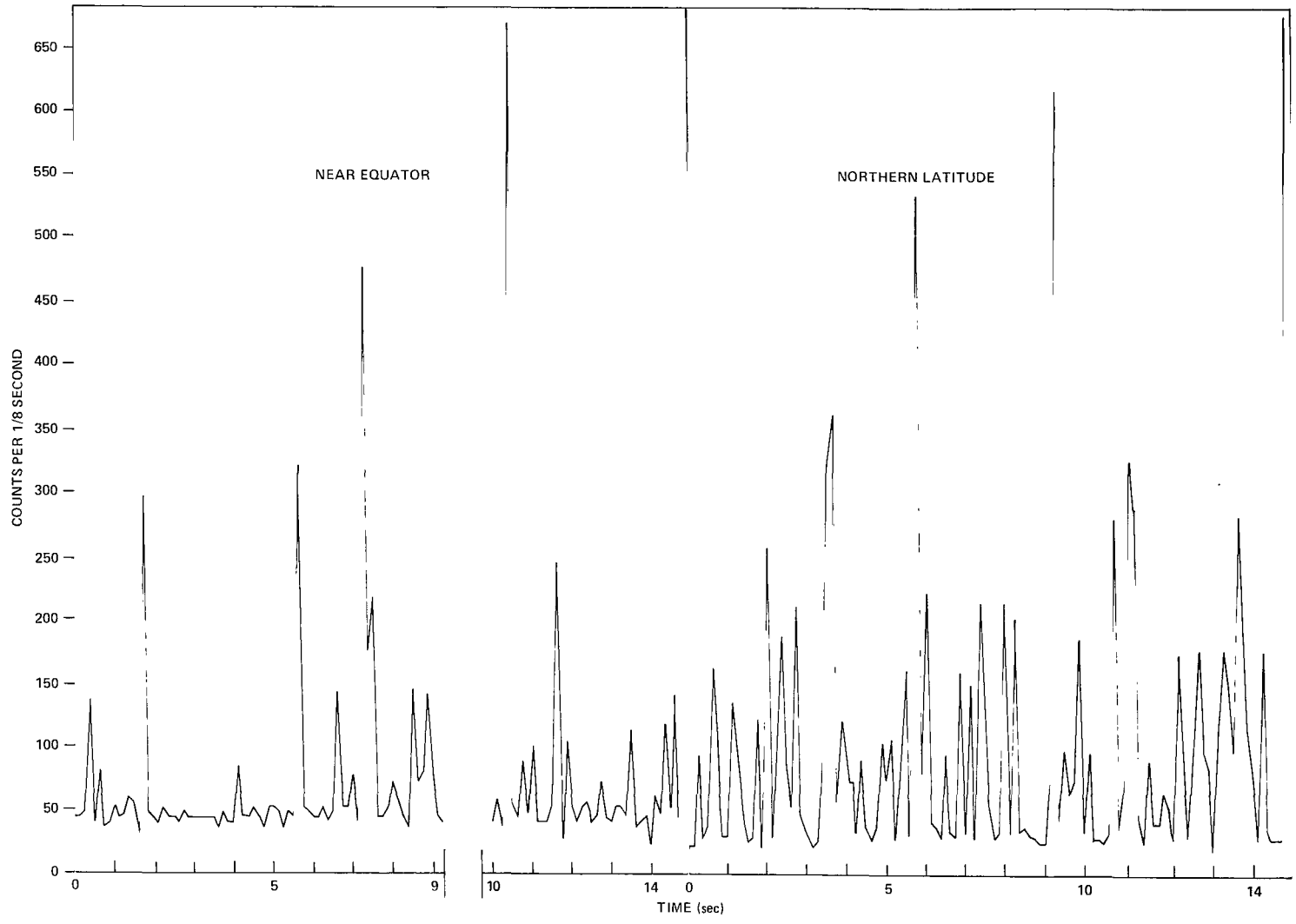

Figure 8. Examples of 1/8-s dark counts of V_1-tube of the Copernicus/Princeton spectrophotometer, taken in orbit #4696 near Equator (left) and in northern latitudes (right).

Under charged-particle radiation, where each independent primary event produces m photoelectrons at a rate, r, leading to an average "dark" count rate, $\overset{\circ}{N}_D = mr$, the standard deviation of the dark counts is $\sigma' = \sqrt{m\overset{\circ}{N}_D t}$, and the signal-to-noise ratio (neglecting thermal counts) becomes:

$$SNR_{Rad} = \frac{\eta \overset{\circ}{N} t}{\sqrt{(\eta \overset{\circ}{N} + m^2 r)t}} \tag{13}$$

Expressing the degradation of the SNR under radiation as the ratio of radiation noise-limited SNR to photon noise-limited SNR, we obtain:

$$\frac{SNR_{Rad}}{SNR_{Ph}} = \left(1 + \frac{m^2 r}{\eta \overset{\circ}{N}}\right)^{-1/2} \tag{14}$$

With appropriate proton-induced dark count rates from figure 6, a window thickness of 1 mm, an average specific energy loss of $\sim$ 1 MeV mm^{-1} for medium energy protons (50 MeV$<$E$<$ 500 MeV), and fluorescence efficiencies from Viehmann et al. (1975), we obtain figure 9, which shows the degradation of SNR as a function of signal photoelectron rate at the peak of the SAA for CsTe, bialkali, and trialkali photocathodes on UV-grade MgF_2 or LiF, respectively. In CsTe end-window tubes at 550 km altitude, SNR is degraded from its photon noise limit for signal rates of $< 10^4$ pe cm^{-2} s^{-1}, for bialkali cathodes below $\sim 3 \cdot 10^5$ pe cm^{-2} s^{-1}, and below $\sim 10^7$ pe cm^{-2} s^{-1} in the case of trialkali cathodes. At 1100 km, corresponding signal rates are about a factor of 10 higher and they are about a decade lower overall for side-window tubes because of the optical decoupling between window and cathode.

Whereas, in the trapped particle belts proton velocities are too low to cause Cerenkov emission and relativistic electrons are removed by moderate amounts of shielding, Cerenkov emission contributes predominantly to the total photoelectron yield per (relativistic) cosmic ray event in trapped radiation-free regions of near-earth orbits, particularly in UV-sensitive tubes. It is important, therefore, to operate phototubes in the counting mode, whenever possible, in order to discriminate against the large Cerenkov pulses and thus effectively reduce the dark current and noise to levels determined by fluorescence. This is illustrated in figure 10, which depicts CR-induced SNR degradation as a function of signal count rate for tubes operated in analog and in pulse counting mode, respectively. In generating these curves we assumed an average charge of Z = 2 (α-particle), a rate of 1 particle cm^{-2} s^{-1} and 1-mm thick windows of MgF_2 or LiF with CsTe, bialkali, and trialkali cathodes, respectively. The m values are taken from figure 4 and in the case of $m_{F\ell}$ are somewhat optimistic in comparison to those found on the Copernicus V-tubes (table 4). This optimism is justified by recent measurements on newly acquired UV-grade MgF_2 samples, which have indicated substantial improvement relative to older material (Viehmann et al.,

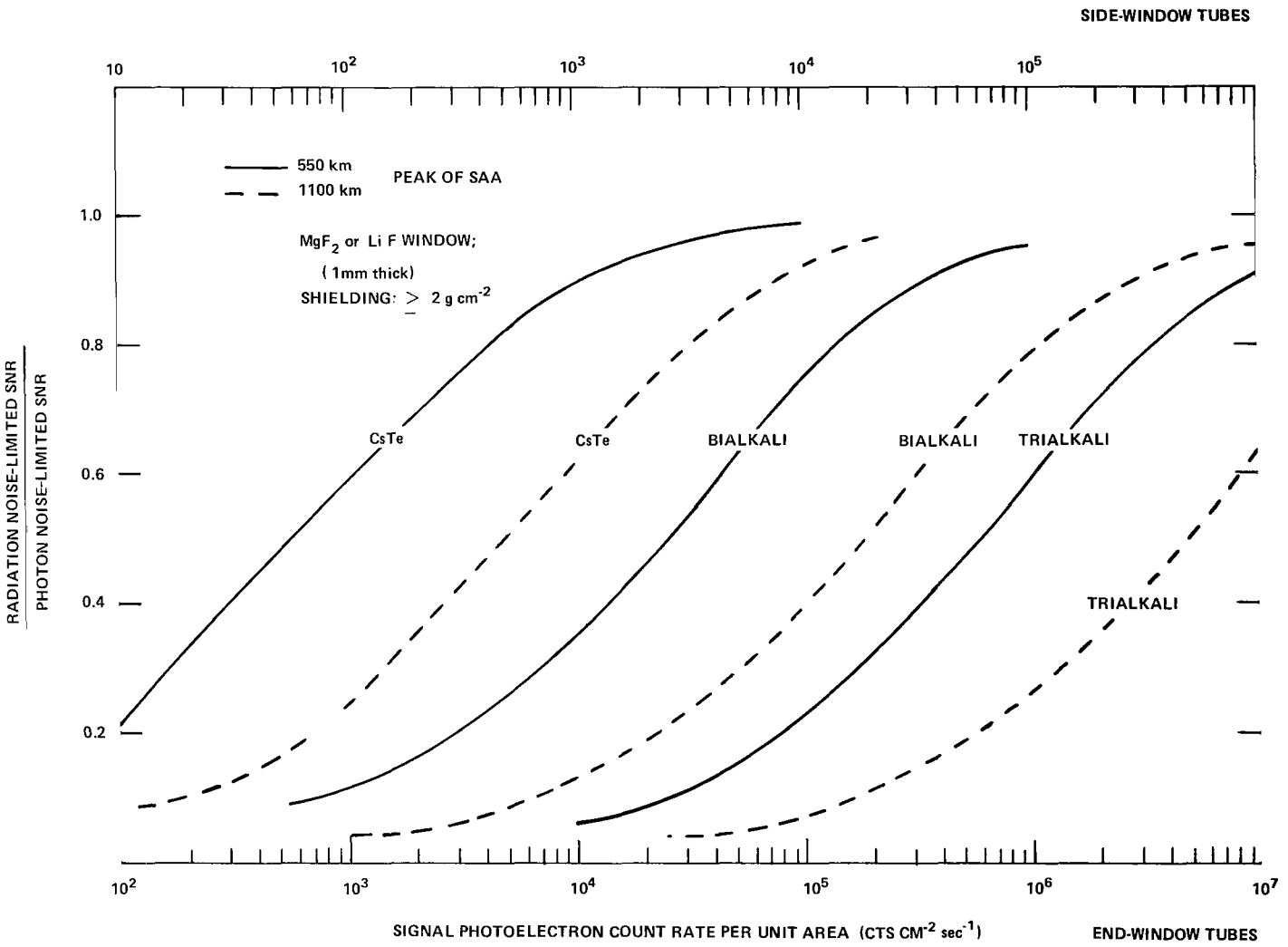

Figure 9. Calculated signal-to-noise degradation in the center of the SAA at 550 km (solid lines) and 1100 km (broken lines) altitude, as a function of signal count rate for multiplier tubes with CsTe, bialkali, and trialkali cathodes on 1-mm thick windows of MgF_2 or LiF.

1975), as well as considerably less susceptibility to radiation damage and, therefore, less increase of fluorescence efficiency with accumulated radiation dose than was experienced on the Copernicus visible sensitive tubes. (The latter would be better represented by the trialkali curves in figure 10.)

The improvement in SNR in the photon counting mode versus analog mode is particularly pronounced in UV-tubes (CsTe) and UV/visible tubes (bialkali), reflecting, of course, the fact that the intensity of Cerenkov emission increases toward shorter wavelength.

To avoid appreciable degradation of SNR from its photon noise limit under galactic cosmic radiation, photon flux densities at end-window detectors (assuming a quantum efficiency of 0.2) should be kept above $\sim 10^2$ photons cm^{-2} s^{-1} for CsTe cathodes, above $\sim 10^3$ photons cm^{-2} s^{-1} for bialkali cathodes, and above $\sim 10^4$ photons cm^{-2} s^{-1} for trialkali cathodes in the photon counting mode. For analog modes, the corresponding flux densities are approximately 100 times higher for CsTe and bialkali and about 10 times higher for trialkali cathodes. Side-window tubes have an advantage of a factor of 10 over end-window tubes.

SUMMARY

Fluorescence and Cerenkov emission resulting from direct interaction of charged particles with the window are by far the dominant mechanisms for radiation-induced noise in multiplier phototubes in space. The photoelectron yields from these primary interactions are orders of magnitude higher than those of "secondary effects" such as bremsstrahlung, phosphorescence (delayed fluorescence), or secondary electron emission. Certain measures can be taken to minimize radiation-induced dark current: Shielding will effectively remove all electrons and low-energy protons (<50 MeV) in trapped radiation belts; the effects of bremsstrahlung produced in the shielding can be neglected in comparison to those of the remaining protons of $E > 50$ MeV, for which shielding becomes impractical. Optical decoupling of window and cathode (side-window tubes) leads to further reduction, as does reducing window thickness and effective cathode area and selection of window/cathode combinations of least efficiency, commensurate with the optical band pass required.

Unlike the conditions in trapped radiation environments, where proton velocities are not high enough to cause Cerenkov emission and relativistic electrons are removed by shielding, Cerenkov emission contributes predominantly to the total photoelectron yield per cosmic-ray event in trapped radiation-free regions of near-earth orbits. It is important, therefore, to operate phototubes in the photon counting mode, in order to discriminate against these large pulses and thus effectively reduce the dark current and noise to levels determined by fluorescence. Optical systems preceding multiplier phototubes should be designed to yield photon flux densities at fully illuminated detector faceplates which exceed the lower limits outlined in figure 10, so as to preclude serious degradation of signal-to-noise ratio from the photon noise limit under cosmic radiation.

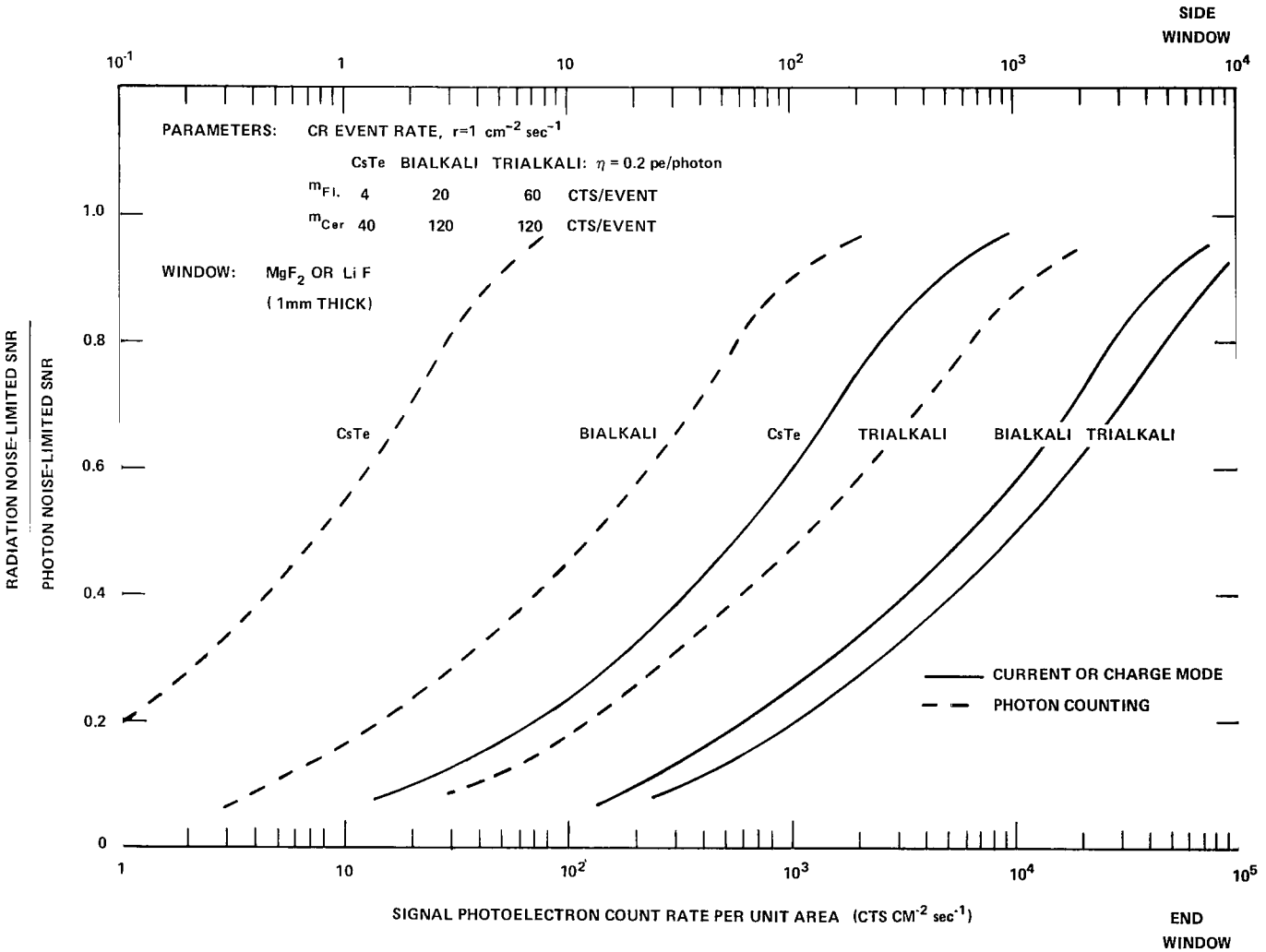

Figure 10. Calculated signal-to-noise degradation of multiplier phototubes under galactic cosmic radiation in photon counting mode (broken curves) and analog mode (solid curves).

ACKNOWLEDGMENTS

The authors thank J. F. Drake and E. Barker (Princeton University Observatory) for making the data in figure 8 available and E. W. Hymowitz (GSFC) for furnishing the ANS data.

Goddard Space Flight Center
National Aeronautics and Space Administration
Greenbelt, Maryland November 1975

REFERENCES

American Institute of Physics Handbook, 2nd Edition, D. Gray, ed., McGraw-Hill Book Co., Inc., New York, 1963.

Birks, J. B., *The Theory and Practice of Scintillation Counting,* Pergamon Press, New York, 1964.

Dressler, K. and L. Spitzer, Jr., "Photomultiplier Tube Pulses Induced by γ Rays," *Rev. Sci. Instr.*, **38**, 1967, p. 436-438.

Evans, R. D., *The Atomic Nucleus,* McGraw-Hill Book Co., Inc., New York, 1955.

Luminescence in Inorganic Solids, P. Goldberg, ed., Academic Press, New York, 1966.

Oda, N., and J. T. Lyman, "Secondary Electron Distribution for Heavy Ions," *Radiation Res. Supplement*, 1967, p. 7, 20.

Rogerson, B., L. Spitzer, J. F. Drake, K. Dressler, E. B. Jenkins, D. C. Morton, and D. G. York, "Spectrophotometric Results from the Copernicus Satellite: I. Instrumentation and Performance," Astrophys. J. (Letters), **181**, 1973.

Viehmann, W., A. G. Eubanks, G. F. Pieper, and J. H. Bredekamp, "Photomultiplier Window Materials under Electron Irradiation, Fluorescence, and Phosphorescence," *Appl. Opt.*, **14**, 1975, p. 2104.

York, D. G., and A. Miller, "Background in Copernicus Tubes," Memorandum to Users of Copernicus Data, Princeton University Observatory, December 9, 1974.

Young, A. T., "Cosmic Ray Induced Dark Current in Photomultipliers," *Rev. Sci. Instr.*, **37**, 1966, p. 1472-1480.

NASA-Langley, 1976

NATIONAL AERONAUTICS AND SPACE ADMINISTRATION
WASHINGTON, D.C. 20546

OFFICIAL BUSINESS
PENALTY FOR PRIVATE USE $300

SPECIAL FOURTH-CLASS RATE
BOOK

POSTAGE AND FEES PAID
NATIONAL AERONAUTICS AND
SPACE ADMINISTRATION
451

U.S.MAIL

POSTMASTER: If Undeliverable (Section 158 Postal Manual) Do Not Return

"The aeronautical and space activities of the United States shall be conducted so as to contribute . . . to the expansion of human knowledge of phenomena in the atmosphere and space. The Administration shall provide for the widest practicable and appropriate dissemination of information concerning its activities and the results thereof."

—NATIONAL AERONAUTICS AND SPACE ACT OF 1958

NASA SCIENTIFIC AND TECHNICAL PUBLICATIONS

TECHNICAL REPORTS: Scientific and technical information considered important, complete, and a lasting contribution to existing knowledge.

TECHNICAL NOTES: Information less broad in scope but nevertheless of importance as a contribution to existing knowledge.

TECHNICAL MEMORANDUMS: Information receiving limited distribution because of preliminary data, security classification, or other reasons. Also includes conference proceedings with either limited or unlimited distribution.

CONTRACTOR REPORTS: Scientific and technical information generated under a NASA contract or grant and considered an important contribution to existing knowledge.

TECHNICAL TRANSLATIONS: Information published in a foreign language considered to merit NASA distribution in English.

SPECIAL PUBLICATIONS: Information derived from or of value to NASA activities. Publications include final reports of major projects, monographs, data compilations, handbooks, sourcebooks, and special bibliographies.

TECHNOLOGY UTILIZATION PUBLICATIONS: Information on technology used by NASA that may be of particular interest in commercial and other non-aerospace applications. Publications include Tech Briefs, Technology Utilization Reports and Technology Surveys.

Details on the availability of these publications may be obtained from:

SCIENTIFIC AND TECHNICAL INFORMATION OFFICE

NATIONAL AERONAUTICS AND SPACE ADMINISTRATION

Washington, D.C. 20546